

ρ^0 Photoproduction in AuAu Collisions at $\sqrt{s_{NN}}=62.4$ GeV with STAR

G. Agakishiev,¹⁷ M. M. Aggarwal,²⁹ Z. Ahammed,⁴⁷ A. V. Alakhverdyants,¹⁷ I. Alekseev,¹⁵ J. Alford,¹⁸ B. D. Anderson,¹⁸ C. D. Anson,²⁷ D. Arkhipkin,² G. S. Averichev,¹⁷ J. Balewski,²² D. R. Beavis,² N. K. Behera,¹³ R. Bellwied,⁴³ M. J. Betancourt,²² R. R. Betts,⁷ A. Bhasin,¹⁶ A. K. Bhati,²⁹ H. Bichsel,⁴⁹ J. Bielcik,⁹ J. Bielcikova,¹⁰ L. C. Bland,² I. G. Bordyuzhin,¹⁵ W. Borowski,⁴⁰ J. Bouchet,¹⁸ E. Braidot,²⁶ A. V. Brandin,²⁵ A. Bridgeman,¹ S. G. Brovko,⁴ E. Bruna,⁵² S. Bueltmann,²⁸ I. Bunzarov,¹⁷ T. P. Burton,² X. Z. Cai,³⁹ H. Caines,⁵² M. Calderón de la Barca Sánchez,⁴ D. Cebra,⁴ R. Cendejas,⁵ M. C. Cervantes,⁴¹ P. Chaloupka,¹⁰ S. Chattopadhyay,⁴⁷ H. F. Chen,³⁷ J. H. Chen,³⁹ J. Y. Chen,⁵¹ L. Chen,⁵¹ J. Cheng,⁴⁴ M. Cherney,⁸ A. Chikhanian,⁵² K. E. Choi,³³ W. Christie,² P. Chung,¹⁰ M. J. M. Coddington,⁴¹ R. Corliss,²² J. G. Cramer,⁴⁹ H. J. Crawford,³ A. Davila Leyva,⁴² L. C. De Silva,⁴³ R. R. Debbes,² T. G. Dedovich,¹⁷ J. Deng,³⁸ A. A. Derevschikov,³¹ R. Derradi de Souza,⁶ L. Didenko,² P. Djawotho,⁴¹ S. M. Dogra,¹⁶ X. Dong,²¹ J. L. Drachenberg,⁴¹ J. E. Draper,⁴ C. M. Du,²⁰ J. C. Dunlop,² L. G. Efimov,¹⁷ M. Elnimr,⁵⁰ J. Engelage,³ G. Eppley,³⁵ M. Estienne,⁴⁰ L. Eun,³⁰ O. Evdokimov,⁷ R. Fatemi,¹⁹ J. Fedorisin,¹⁷ R. G. Fersch,¹⁹ P. Filip,¹⁷ E. Finch,⁵² V. Fine,² Y. Fisyak,² C. A. Gagliardi,⁴¹ F. Geurts,³⁵ P. Ghosh,⁴⁷ Y. N. Gorbunov,⁸ A. Gordon,² O. G. Grebenyuk,²¹ D. Grosnick,⁴⁶ A. Gupta,¹⁶ S. Gupta,¹⁶ W. Guryn,² B. Haag,⁴ O. Hajkova,⁹ A. Hamed,⁴¹ L-X. Han,³⁹ J. W. Harris,⁵² J. P. Hays-Wehle,²² M. Heinz,⁵² S. Heppelmann,³⁰ A. Hirsch,³² E. Hjort,²¹ G. W. Hoffmann,⁴² D. J. Hofman,⁷ B. Huang,³⁷ H. Z. Huang,⁵ T. J. Humanic,²⁷ L. Huo,⁴¹ G. Igo,⁵ P. Jacobs,²¹ W. W. Jacobs,¹⁴ C. Jena,¹² F. Jin,³⁹ J. Joseph,¹⁸ E. G. Judd,³ S. Kabana,⁴⁰ K. Kang,⁴⁴ J. Kapitan,¹⁰ K. Kauder,⁷ H. W. Ke,⁵¹ D. Keane,¹⁸ A. Kechechyan,¹⁷ D. Kettler,⁴⁹ D. P. Kikola,³² J. Kiryluk,²¹ A. Kisiel,⁴⁸ V. Kizka,¹⁷ S. R. Klein,²¹ A. G. Knospe,⁵² D. D. Koetke,⁴⁶ T. Kollegger,¹¹ J. Konzer,³² I. Koralt,²⁸ L. Koroleva,¹⁵ W. Korsch,¹⁹ L. Kotchenda,²⁵ V. Kouchpil,¹⁰ P. Kravtsov,²⁵ K. Krueger,¹ M. Krus,⁹ L. Kumar,¹⁸ M. A. C. Lamont,² J. M. Landgraf,² S. LaPointe,⁵⁰ J. Lauret,² A. Lebedev,² R. Lednicky,¹⁷ J. H. Lee,² W. Leight,²² M. J. LeVine,² C. Li,³⁷ L. Li,⁴² N. Li,⁵¹ W. Li,³⁹ X. Li,³² X. Li,³⁸ Y. Li,⁴⁴ Z. M. Li,⁵¹ L. M. Lima,³⁶ M. A. Lisa,²⁷ F. Liu,⁵¹ H. Liu,⁴ J. Liu,³⁵ T. Ljubicic,² W. J. Llope,³⁵ R. S. Longacre,² Y. Lu,³⁷ E. V. Lukashov,²⁵ X. Luo,³⁷ G. L. Ma,³⁹ Y. G. Ma,³⁹ D. P. Mahapatra,¹² R. Majka,⁵² O. I. Mall,⁴ R. Manweiler,⁴⁶ S. Margetis,¹⁸ C. Markert,⁴² H. Masui,²¹ H. S. Matis,²¹ D. McDonald,³⁵ T. S. McShane,⁸ A. Meschanin,³¹ R. Milner,²² N. G. Minaev,³¹ S. Mioduszewski,⁴¹ M. K. Mitrovski,² Y. Mohammed,⁴¹ B. Mohanty,⁴⁷ M. M. Mondal,⁴⁷ B. Morozov,¹⁵ D. A. Morozov,³¹ M. G. Munhoz,³⁶ M. K. Mustafa,³² M. Naglis,²¹ B. K. Nandi,¹³ T. K. Nayak,⁴⁷ L. V. Nogach,³¹ S. B. Nurushev,³¹ G. Odyniec,²¹ A. Ogawa,² K. Oh,³³ A. Ohlson,⁵² V. Okorokov,²⁵ E. W. Oldag,⁴² R. A. N. Oliveira,³⁶ D. Olson,²¹ M. Pachr,⁹ B. S. Page,¹⁴ S. K. Pal,⁴⁷ Y. Pandit,¹⁸ Y. Panebratsev,¹⁷ T. Pawlak,⁴⁸ H. Pei,⁷ T. Peitzmann,²⁶ C. Perkins,³ W. Peryt,⁴⁸ P. Pile,² M. Planinic,⁵³ M. A. Ploskon,²¹ J. Pluta,⁴⁸ D. Plyku,²⁸ N. Poljak,⁵³ J. Porter,²¹ A. M. Poskanzer,²¹ B. V. K. S. Potukuchi,¹⁶ C. B. Powell,²¹ D. Prindle,⁴⁹ C. Pruneau,⁵⁰ N. K. Pruthi,²⁹ P. R. Pujahari,¹³ J. Putschke,⁵² H. Qiu,²⁰ R. Raniwala,³⁴ S. Raniwala,³⁴ R. L. Ray,⁴² R. Redwine,²² R. Reed,⁴ H. G. Ritter,²¹ J. B. Roberts,³⁵ O. V. Rogachevskiy,¹⁷ J. L. Romero,⁴ L. Ruan,² J. Rusnak,¹⁰ N. R. Sahoo,⁴⁷ I. Sakrejda,²¹ S. Salur,⁴ J. Sandweiss,⁵² E. Sangaline,⁴ A. Sarkar,¹³ J. Schambach,⁴² R. P. Scharenberg,³² J. Schaub,⁴⁶ A. M. Schmah,²¹ N. Schmitz,²³ T. R. Schuster,¹¹ J. Seele,²² J. Seger,⁸ I. Selyuzhenkov,¹⁴ P. Seyboth,²³ N. Shah,⁵ E. Shahaliev,¹⁷ M. Shao,³⁷ M. Sharma,⁵⁰ S. S. Shi,⁵¹ Q. Y. Shou,³⁹ E. P. Sichtermann,²¹ F. Simon,²³ R. N. Singaraju,⁴⁷ M. J. Skoby,³² N. Smirnov,⁵² D. Solanki,³⁴ P. Sorensen,² U. G. deSouza,³⁶ H. M. Spinka,¹ B. Srivastava,³² T. D. S. Stanislaus,⁴⁶ S. G. Steadman,²² J. R. Stevens,¹⁴ R. Stock,¹¹ M. Strikhanov,²⁵ B. Stringfellow,³² A. A. P. Suaide,³⁶ M. C. Suarez,⁷ N. L. Subba,¹⁸ M. Sumbera,¹⁰ X. M. Sun,²¹ Y. Sun,³⁷ Z. Sun,²⁰ B. Surrow,²² D. N. Svirida,¹⁵ T. J. M. Symons,²¹ A. Szanto de Toledo,³⁶ J. Takahashi,⁶ A. H. Tang,² Z. Tang,³⁷ L. H. Tarini,⁵⁰ T. Tarnowsky,²⁴ D. Thein,⁴² J. H. Thomas,²¹ J. Tian,³⁹ A. R. Timmins,⁴³ D. Tlusty,¹⁰ M. Tokarev,¹⁷ T. A. Trainor,⁴⁹ S. Trentalange,⁵ R. E. Tribble,⁴¹ P. Tribedy,⁴⁷ B. A. Trzeciak,⁴⁸ O. D. Tsai,⁵ T. Ullrich,² D. G. Underwood,¹ G. Van Buren,² G. van Nieuwenhuizen,²² J. A. Vanfossen, Jr.,¹⁸ R. Varma,¹³ G. M. S. Vasconcelos,⁶ A. N. Vasiliev,³¹ F. Videbæk,² Y. P. Vijoyi,⁴⁷ S. Vokal,¹⁷ S. A. Voloshin,⁵⁰ M. Wada,⁴² M. Walker,²² F. Wang,³² G. Wang,⁵ H. Wang,²⁴ J. S. Wang,²⁰ Q. Wang,³² X. L. Wang,³⁷ Y. Wang,⁴⁴ G. Webb,¹⁹ J. C. Webb,² G. D. Westfall,²⁴ C. Whitten Jr.,^{5, *} H. Wieman,²¹ S. W. Wissink,¹⁴ R. Witt,⁴⁵ W. Witzke,¹⁹ Y. F. Wu,⁵¹ Z. Xiao,⁴⁴ W. Xie,³² H. Xu,²⁰ N. Xu,²¹ Q. H. Xu,³⁸ W. Xu,⁵ Y. Xu,³⁷ Z. Xu,² L. Xue,³⁹ Y. Yang,²⁰ Y. Yang,⁵¹ P. Yepes,³⁵ K. Yip,² I-K. Yoo,³³ M. Zawisza,⁴⁸ H. Zbroszczyk,⁴⁸ W. Zhan,²⁰ J. B. Zhang,⁵¹ S. Zhang,³⁹ W. M. Zhang,¹⁸ X. P. Zhang,⁴⁴ Y. Zhang,²¹ Z. P. Zhang,³⁷ F. Zhao,⁵ J. Zhao,³⁹ C. Zhong,³⁹ X. Zhu,⁴⁴ Y. H. Zhu,³⁹ and Y. Zoulkarneeva¹⁷

(STAR Collaboration)

- ¹Argonne National Laboratory, Argonne, Illinois 60439, USA
²Brookhaven National Laboratory, Upton, New York 11973, USA
³University of California, Berkeley, California 94720, USA
⁴University of California, Davis, California 95616, USA
⁵University of California, Los Angeles, California 90095, USA
⁶Universidade Estadual de Campinas, Sao Paulo, Brazil
⁷University of Illinois at Chicago, Chicago, Illinois 60607, USA
⁸Creighton University, Omaha, Nebraska 68178, USA
⁹Czech Technical University in Prague, FNSPE, Prague, 115 19, Czech Republic
¹⁰Nuclear Physics Institute AS CR, 250 68 Řež/Prague, Czech Republic
¹¹University of Frankfurt, Frankfurt, Germany
¹²Institute of Physics, Bhubaneswar 751005, India
¹³Indian Institute of Technology, Mumbai, India
¹⁴Indiana University, Bloomington, Indiana 47408, USA
¹⁵Alikhanov Institute for Theoretical and Experimental Physics, Moscow, Russia
¹⁶University of Jammu, Jammu 180001, India
¹⁷Joint Institute for Nuclear Research, Dubna, 141 980, Russia
¹⁸Kent State University, Kent, Ohio 44242, USA
¹⁹University of Kentucky, Lexington, Kentucky, 40506-0055, USA
²⁰Institute of Modern Physics, Lanzhou, China
²¹Lawrence Berkeley National Laboratory, Berkeley, California 94720, USA
²²Massachusetts Institute of Technology, Cambridge, MA 02139-4307, USA
²³Max-Planck-Institut für Physik, Munich, Germany
²⁴Michigan State University, East Lansing, Michigan 48824, USA
²⁵Moscow Engineering Physics Institute, Moscow Russia
²⁶NIKHEF and Utrecht University, Amsterdam, The Netherlands
²⁷Ohio State University, Columbus, Ohio 43210, USA
²⁸Old Dominion University, Norfolk, VA, 23529, USA
²⁹Panjab University, Chandigarh 160014, India
³⁰Pennsylvania State University, University Park, Pennsylvania 16802, USA
³¹Institute of High Energy Physics, Protvino, Russia
³²Purdue University, West Lafayette, Indiana 47907, USA
³³Pusan National University, Pusan, Republic of Korea
³⁴University of Rajasthan, Jaipur 302004, India
³⁵Rice University, Houston, Texas 77251, USA
³⁶Universidade de Sao Paulo, Sao Paulo, Brazil
³⁷University of Science & Technology of China, Hefei 230026, China
³⁸Shandong University, Jinan, Shandong 250100, China
³⁹Shanghai Institute of Applied Physics, Shanghai 201800, China
⁴⁰SUBATECH, Nantes, France
⁴¹Texas A&M University, College Station, Texas 77843, USA
⁴²University of Texas, Austin, Texas 78712, USA
⁴³University of Houston, Houston, TX, 77204, USA
⁴⁴Tsinghua University, Beijing 100084, China
⁴⁵United States Naval Academy, Annapolis, MD 21402, USA
⁴⁶Valparaiso University, Valparaiso, Indiana 46383, USA
⁴⁷Variable Energy Cyclotron Centre, Kolkata 700064, India
⁴⁸Warsaw University of Technology, Warsaw, Poland
⁴⁹University of Washington, Seattle, Washington 98195, USA
⁵⁰Wayne State University, Detroit, Michigan 48201, USA
⁵¹Institute of Particle Physics, CCNU (HZNU), Wuhan 430079, China
⁵²Yale University, New Haven, Connecticut 06520, USA
⁵³University of Zagreb, Zagreb, HR-10002, Croatia

(Dated: January 22, 2022)

Vector mesons may be photoproduced in relativistic heavy-ion collisions when a virtual photon emitted by one nucleus scatters from the other nucleus, emerging as a vector meson. The STAR Collaboration has previously presented measurements of coherent ρ^0 photoproduction at center of mass energies of 130 GeV and 200 GeV in AuAu collisions. Here, we present a measurement of the cross section at 62.4 GeV; we find that the cross section for coherent ρ^0 photoproduction with nuclear breakup is $10.5 \pm 1.5 \pm 1.6$ mb at 62.4 GeV. The cross-section ratio between 200 GeV and 62.4 GeV is 4.4 ± 0.6 , less than is predicted by most theoretical models. It is, however, proportionally much larger than the previously observed $15\% \pm 55\%$ increase between 130 GeV and 200 GeV.

I. INTRODUCTION

When nuclei cross paths at impact parameters b larger than twice the nuclear radius, R_A , they can interact electromagnetically rather than hadronically. Such events are referred to as Ultra Peripheral Collisions (UPCs). The coupling between these relativistic nuclei is based on the Weizsäcker-Williams formalism [1], where their highly boosted electromagnetic fields are modeled by a flux of photons with small virtuality [2]. The photon flux scales as the square of the nuclear charge and reaches very high values in ions with large atomic number. The interaction between the photon flux and nuclear matter is described with an intermediate fluctuation of the photons into quark antiquark dipoles ($q\bar{q}$) which then scatter from the other nucleus and may emerge as a vector meson. The production cross section of the vector meson depends on the $q\bar{q}$ coupling to the nuclear target. At small transverse momentum, $p_T < \hbar/R_A$, the $q\bar{q}$ pair couples coherently to the entire nucleus. Incoherent coupling takes place at higher p_T where the dipole interacts with individual nucleons. The high photon flux allows for several photon exchanges per event. Real photons excite giant dipole resonances or higher excitation states in the other nucleus which then usually emit one or more neutrons [2] in the beam direction which in turn can be used to trigger on these UPC events.

Four models provide a description of the coherent vector meson production in UPC heavy ion interactions. The first one, which we will refer to as KN (Klein and Nystrand) is based on vector meson dominance (VMD) and a classical-mechanical Glauber approach for nuclear scattering [3]. The second model, named FSZ (Frankfurt, Strikman and Zhilov), makes use of a generalized VMD formalism and a QCD Gribov-Glauber approach [4, 5]. The third model IIM-GM (Iancu, Itakura, Munier - Goncalves, Machado) utilizes a QCD color dipole formalism and includes nuclear effects and parton saturation phenomena [6, 7]. The fourth model IPSAT-GM (Impact Parameter Saturation - Goncalves and Machado) is based on the third one but it also includes the impact parameter dependence of the dipole interaction with the target nucleus and DGLAP evolution [8] for the target gluon distribution [9].

The STAR collaboration has previously measured the coherent ρ^0 photoproduction in AuAu collisions at center of mass per nucleon-pair energies $\sqrt{s_{NN}} = 130$ and 200 GeV [10, 11]. STAR observed a rather small energy dependence, with only about a 15% \pm 55% increase in total cross section between the two beam energies. In contrast, both Glauber models (KN and FSZ) predict about a 60% rise in cross section; the two saturation models predict a somewhat slower increase, about 30% and 33% respectively. Here, we present results obtained at a lower energy of $\sqrt{s_{NN}} = 62.4$ GeV to further study the energy-dependence of the cross section. We measured the cross section for coherent exclusive ρ^0 photoproduction accompanied by mutual Coulomb excitation of the beam ions and compare the measured cross section with available theoretical models.

II. EXPERIMENTAL SETUP AND TRIGGERING

The analysis reported here is based on data collected with the STAR detector from AuAu collisions at $\sqrt{s_{NN}} = 62.4$ GeV at the Relativistic Heavy Ion Collider at Brookhaven National Laboratory. Charged particles emerging from those interactions have been detected with the cylindrical Time Projection Chamber (TPC) [12]. The TPC detected charged tracks with pseudorapidity $|\eta| < 1.2$ and transverse momentum $p_T > 100$ MeV/c, with an overall efficiency of about 85%. At the time these data were collected, the TPC was surrounded by the 240 scintillator slats forming the Central Trigger Barrel (CTB) [13]. Two Zero Degree hadron Calorimeters (ZDCs) [14] are situated along the beam pipe at ± 18 m downstream from the interaction point. The ZDCs have an acceptance close to unity for neutrons originating from nuclear break-up.

The data were collected with two slightly different minimum bias triggers. Both triggers required that the energy in each ZDC be greater than zero, so were sensitive to ρ^0 photoproduction accompanied by mutual Coulomb excitation, while eliminating most cosmic-ray muons, beam-gas interactions and non beam-beam events. For the first trigger, trigger A, this was the only requirement. The second trigger, trigger B, also required that charged particles be detected in the CTB, eliminating empty events, such as those caused by interactions consisting of only mutual Coulomb association. This trigger had a lower rate, so it was more efficient and could be run with a lower prescale.

*Deceased

The data selection criteria applied in this analysis followed closely the ones used in previous STAR ρ^0 photoproduction analyses [10, 11]; events should have two oppositely charged tracks, each with more than 14 out of 45 possible hits in the TPC, and both tracks should originate from a common vertex near the interaction region. Vertexing efficiency at the level of two tracks has been found to be as high as 80 % [15].

There are several types of backgrounds to ρ^0 photoproduction: peripheral hadronic interactions, other photonuclear interactions, e^+e^- pairs from two-photon interactions [16], and processes such as beam-gas interactions, cosmic ray muons and pile-up events. Those events have been suppressed by selecting events originating from within a cylindrical region of 15 cm radius and 100 cm longitudinal extension centered at the primary interaction point and containing a ρ^0 meson candidate with transverse momentum less than 150 MeV/c. As was the case in previous UPC STAR analyses [10, 11], the contribution from e^+e^- pairs was found to be negligible, and no particle identification was needed in this analysis due to the low level of background.

The geometrical acceptance and the reconstruction efficiency have been studied with the help of a Monte Carlo event generator based on the KN model [17]. Simulated ρ^0 photoproduction events have been used as input to the standard STAR detector Monte-Carlo simulation. The KN model reproduces the kinematic features of photoproduced ρ^0 [17], while the detector simulation has been well-tested on central hadronic collisions. The simulated ρ^0 were then embedded into data collected with a zero-bias trigger (beam bunch crossing-time trigger). This procedure incorporates the effects of additional tracks, which are present in the data as a result of event pile-up and noise in the STAR TPC.

The ρ^0 total reconstruction efficiency has been studied as a function of transverse momentum, rapidity, invariant mass and azimuthal and polar angles for each of the two trigger implementations. Within the rapidity window $|y_{\rho^0}| < 1$, the mean reconstruction efficiency for the data set collected with trigger A is 36 ± 3 % whereas the dataset collected with trigger B is 9 ± 1 %. The reconstruction efficiencies are relatively constant as functions of transverse momentum, invariant mass, azimuthal and polar angle but slowly decrease at higher rapidity ($|y_{\rho^0}| > 1$), due to the TPC acceptance [15].

III. ρ^0 PHOTOPRODUCTION

The sampled luminosity has been determined based on the assumption that the main contribution to the total cross section comes from hadronic production with a well known cross section. The luminosity was measured by counting the number of events with more than 313 tracks in the TPC within $|y| \leq 0.5$ and with at least ten hits per track. These criteria select 10 % of the total hadronic cross section [18]. The final measured integrated luminosity for the data selected with trigger A is 45 mb^{-1} and for the one accumulated with trigger B is 781 mb^{-1} . The systematic uncertainty for the measured integrated luminosity is 10 % [10]. Due to the limited luminosity sampled with trigger A, all results in this publication are based on data obtained with trigger B unless mentioned otherwise.

The invariant mass distributions have been obtained with pairs of opposite-sign charge tracks assumed to be pions pointing to neutral two-track vertices. The resulting efficiency corrected invariant mass distributions are shown in Fig. 1 for the data sets collected with trigger A (left) and trigger B (right).

Pion pair photoproduction occurs through two main channels: pairs are produced by the decay of a ρ^0 meson, or by a photon fluctuating directly into a $\pi^+\pi^-$ pair, which has a flat $M_{\pi^+\pi^-}$ distribution. These two distributions of pion pairs interfere constructively for $M_{\pi^+\pi^-} < M_{\rho^0}$ and destructively for $M_{\pi^+\pi^-} > M_{\rho^0}$.

Random combinatoric background comes mostly from peripheral AuAu hadronic interactions. For the coherently produced ρ^0 mesons, the combinatorial background has been estimated with the help of like-sign pairs ($\pi^+\pi^+$ and $\pi^-\pi^-$) and scaled by a factor of 2.2 ± 0.1 to match the unlike pair spectra at high transverse momentum, $p_T \geq 250 \text{ MeV}/c$. The transverse momentum distribution of ρ^0 candidates along with the scaled combinatorial background are shown in Fig. 2. For comparison, we also estimated the background with high multiplicity events. The different methods of background estimation gave cross sections which differ by less than 3 %.

The invariant mass distribution has been fitted with a relativistic Breit-Wigner function plus a term describing the direct $\pi^+\pi^-$ production and its interference with the ρ^0 (Söding term) [19]. In addition, a background term was added which was approximated by a second order polynomial. The total fit function then reads:

$$\frac{dN}{dM_{\pi^+\pi^-}} = \left| A_{\rho^0} \frac{\sqrt{M_{\pi^+\pi^-} - M_{\rho^0}} \Gamma_{\rho^0}}{M_{\pi^+\pi^-}^2 - M_{\rho^0}^2 + iM_{\rho^0} \Gamma_{\rho^0}} + A_{\pi\pi} \right|^2 + f_p, \quad (1)$$

where the amplitudes for the ρ^0 and direct pion pairs are A_{ρ^0} and $A_{\pi\pi}$ respectively, and f_p is the fixed second order polynomial which describes the background. The width and mass obtained from the fit to the invariant mass distribution based on the dataset collected with trigger B are $M_{\rho^0} = 0.764 \pm 0.009 \text{ GeV}/c^2$ and $\Gamma_{\rho^0} = 0.140 \pm 0.013 \text{ GeV}/c^2$ which is consistent with current world average (Particle Data Group (PDG)) [20] values for photoproduced ρ^0 of $M_{\rho^0}^{PDG} = 0.7685 \pm 0.0011 \text{ GeV}/c^2$ and $\Gamma_{\rho^0}^{PDG} = 0.1507 \pm 0.0029 \text{ GeV}/c^2$.

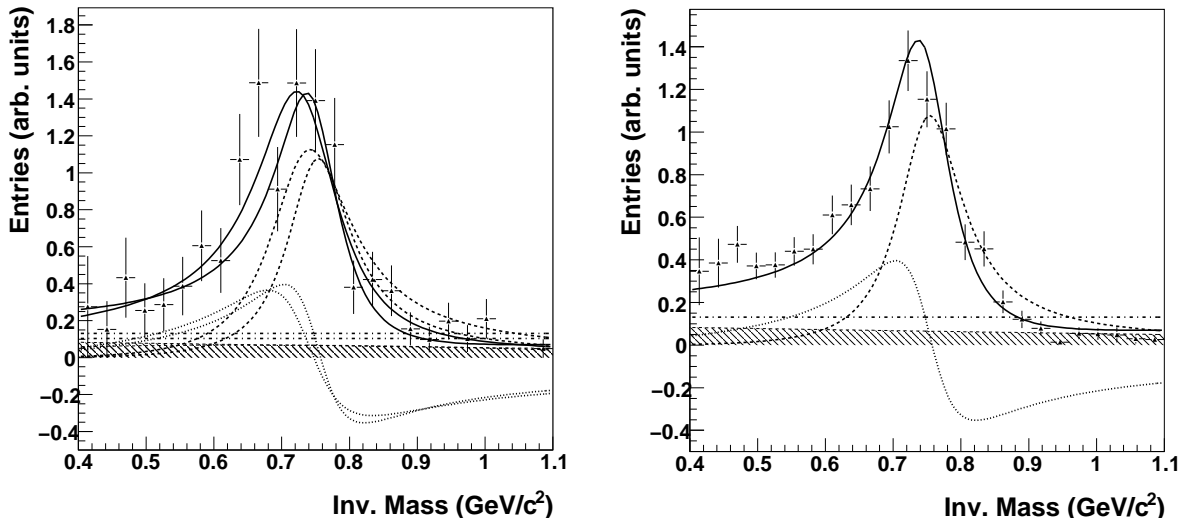


FIG. 1: Acceptance corrected invariant mass distributions for the coherently produced ρ^0 candidates collected with trigger A (left) and B (right). The fit function (solid) encompasses the Breit-Wigner (dashed), the mass independent contribution from direct $\pi^+\pi^-$ production (dash-dotted), and the interference term (dotted). The hatched area is the contribution from the combinatorial background. The statistical errors are shown.

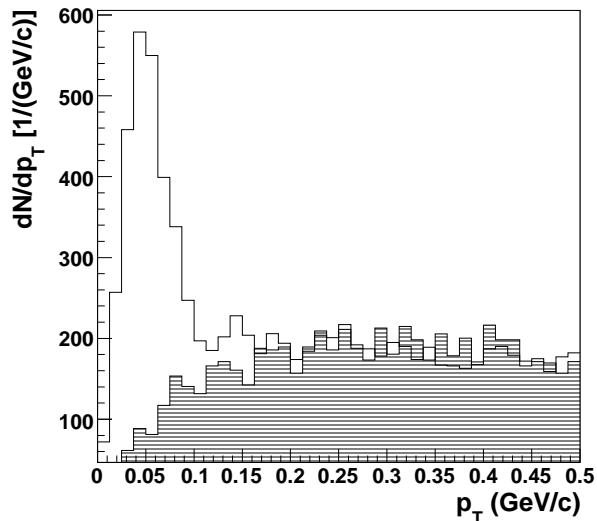


FIG. 2: Transverse momentum distribution of the ρ^0 candidates (open distribution) overlaid by the combinatorial background estimated with like-sign pairs (not corrected to the acceptance and reconstruction efficiency) and scaled to match in the high transverse momentum region, $p_T \geq 250$ MeV/c (hatched distribution). The plot is based on the dataset collected with trigger B.

The fit function allows a measurement of the ratio of the Breit-Wigner amplitude (A_{ρ^0}) to the amplitude for the direct $\pi^+\pi^-$ production ($A_{\pi\pi}$). The measured $|A_{\pi\pi}/A_{\rho^0}| = 0.88 \pm 0.09$ (stat.) ± 0.09 (syst.) $(\text{GeV}/c^2)^{-1/2}$. This is in agreement with previous STAR measurements of the ratio: 0.81 ± 0.08 (stat.) ± 0.20 (syst.) $(\text{GeV}/c^2)^{-1/2}$ at $\sqrt{s_{NN}} = 130$ GeV and 0.89 ± 0.08 (stat.) ± 0.09 (syst.) $(\text{GeV}/c^2)^{-1/2}$ at $\sqrt{s_{NN}} = 200$ GeV. The systematic errors on the fits are determined by varying the fit function (for example, by fixing the ρ^0 mass to the PDG value, or by varying the fitting range and changing the binning of the invariant mass distribution).

Figure 3 shows the ρ^0 differential production cross section as a function of $t = p_T^2$, averaged over rapidity in the $|y_{\rho^0}| < 1$ window. The distribution was obtained by fitting invariant mass distributions for each t bin with Eq. 1 in order to extract the ρ^0 yield. The $d^2\sigma/dydt$ distribution is fit with the sum of two exponential terms (see Eq. 5

TABLE I: Parameters for the fit to the $d^2\sigma/dydt$.

Parameter	
A_{coh}	$1328 \pm 159 \text{ mb}/(\text{GeV}/c)^2$
B_{coh}	$257 \pm 32 (\text{GeV}/c)^{-2}$
A_{inc}	$22.8 \pm 15.3 \text{ mb}/(\text{GeV}/c)^2$
B_{inc}	$21.6 \pm 11.4 (\text{GeV}/c)^{-2}$

of Ref. [10]) representing the coherent (small values of t) and the incoherent photoproduction (which dominates for $t > 0.02 \text{ GeV}^2/c^2$). The combinatorial background was described by the unscaled like-sign pairs in order to retain the incoherent ρ^0 signal. The measured slope for the coherent photoproduction is $B_{\text{coh}} = 257 \pm 32 (\text{GeV}/c)^{-2}$ and the slope for the incoherent photoproduction is $B_{\text{inc}} = 21.6 \pm 11.4 (\text{GeV}/c)^{-2}$. Both are in agreement with previously published STAR measurements [10]. The fit was used to determine the ratio of the incoherent to coherent production cross sections $\sigma_{\text{incoherent}}/\sigma_{\text{coherent}} = 0.20 \pm 0.08$ (stat.) ± 0.08 (syst.) for $|y_{\rho^0}| < 1$. This is about 1σ lower than the measurement $\sigma_{\text{incoherent}}/\sigma_{\text{coherent}} = 0.29 \pm 0.03$ (stat.) ± 0.08 (syst.) at $\sqrt{s_{NN}} = 200 \text{ GeV}$ [10].

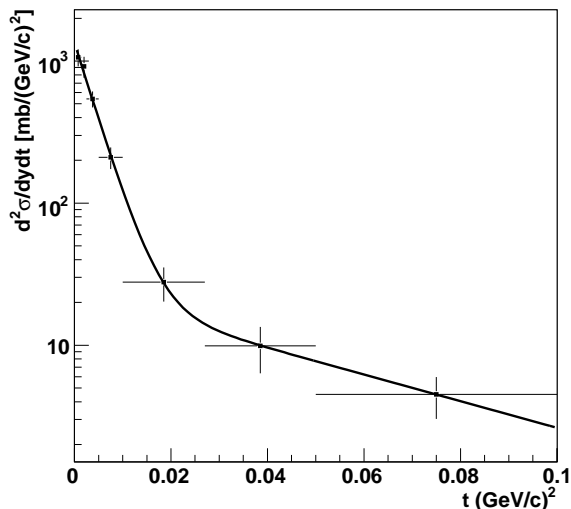


FIG. 3: ρ^0 production cross section determined with the data set collected with trigger B, as a function of momentum transfer t , fitted with a double exponential fit function in the range $t < 0.1$. The statistical errors are shown. The ratio of incoherent to coherent cross sections is measured to be 0.20 ± 0.8 . The fit parameters are shown in Table I.

The final cross section numbers involve extrapolation from the observed $|y_{\rho^0}| < 1$ to all rapidity, and also corrections to account for the presence or absence of accompanying nuclear excitation. The cross section for coherent production accompanied by mutual nuclear excitation in the $|y_{\rho^0}| < 1$ window, measured with data collected with Trigger B, is $\sigma_{\text{coh}}(XnXn, |y_{\rho^0}| < 1) = 6.2 \pm 0.9$ (stat.) ± 0.8 (syst.) mb. From this, one can infer the cross section in this same rapidity window for coherent production accompanied by the excitation of only a single nucleus, and also for coherent production with no accompanying excitation. This is done using the ratios $\sigma(0n0n)/\sigma(XnXn)$ and $\sigma(0nXn)/\sigma(XnXn)$, where $*n$ represents the number of neutrons detected in each ZDC. These ratios were measured by the STAR collaboration at $\sqrt{s_{NN}} = 200 \text{ GeV}$ [10] and proved to be in good agreement with those predicted by STARlight. STARlight is a Monte Carlo that simulates two-photon and photon-Pomeron interactions between relativistic nuclei [21]. Assuming similar agreement, the ratios predicted by STARlight at $\sqrt{s_{NN}} = 62 \text{ GeV}$, $\sigma(0n0n)/\sigma(XnXn) = 4.6 \pm 0.5$ (syst.) and $\sigma(0nXn)/\sigma(XnXn) = 2.7 \pm 0.2$ (syst.), are used to extrapolate the current data. The coherent production cross section with a single nuclear excitation in the $|y_{\rho^0}| < 1$ window is then $\sigma_{\text{coh}}(0nXn, |y_{\rho^0}| < 1) = 16.7 \pm 2.7$ (stat.) ± 2.0 (syst.) mb, and the coherent production cross section with no accompanying excitation in the $|y_{\rho^0}| < 1$ window is $\sigma_{\text{coh}}(0n0n, |y_{\rho^0}| < 1) = 28.5 \pm 5.2$ (stat.) ± 4.8 (syst.) mb.

The extrapolation factors to obtain the cross sections over the full rapidity range are model dependent. Using the KN model [10, 22], this factor was estimated to be 1.7 ± 0.1 for events accompanied by nuclear excitation, 1.9 ± 0.1 for events accompanied by a single nuclear excitation, and 2.7 ± 0.1 for events with no accompanying excitation. It

TABLE II: The total cross section extrapolated to the full rapidity range for coherent ρ^0 production at $\sqrt{s_{NN}} = 62.4$ GeV accompanied by nuclear breakup and without breakup, compared with previous measurements at 130 GeV and 200 GeV [10, 11]. The measured cross section, for XnXn events with $|y_{\rho^0}| < 1$, is based on the dataset collected with trigger B. Cross sections for other levels of nuclear excitation, and for the full rapidity range, are calculated with extrapolation factors detailed in the text. Statistical and systematic errors are shown.

Parameter	STAR at	STAR at	STAR at	STAR at
	$\sqrt{s_{NN}} = 62.4$ GeV coherent ($ y_{\rho^0} < 1$)	$\sqrt{s_{NN}} = 62.4$ GeV coherent (full rapidity)	$\sqrt{s_{NN}} = 130$ GeV [11] coherent (full rapidity)	$\sqrt{s_{NN}} = 200$ GeV [10] coherent (full rapidity)
$\sigma_{XnXn}^{\rho^0}$ (mb)	$6.2 \pm 0.9 \pm 0.8$	$10.5 \pm 1.5 \pm 1.6$	$28.3 \pm 2.0 \pm 6.3$	$31.9 \pm 1.5 \pm 4.5$
$\sigma_{0nXn}^{\rho^0}$ (mb)	$16.7 \pm 2.7 \pm 2.$	$31.8 \pm 5.2 \pm 3.9$	$95 \pm 60 \pm 25$	$105 \pm 5 \pm 15$
$\sigma_{0n0n}^{\rho^0}$ (mb)	$28.5 \pm 5.2 \pm 4.8$	$78 \pm 14 \pm 13$	$370 \pm 170 \pm 80$	$391 \pm 18 \pm 55$
$\sigma_{total}^{\rho^0}$ (mb)	$51.5 \pm 5.9 \pm 5.3$	$120 \pm 15 \pm 22$	$460 \pm 220 \pm 110$	$530 \pm 19 \pm 57$

is worth noting that, per Fig. 7 of Ref. [10], different models predict rather different extrapolation factors, and the IPOSAT and IIM models would have a considerably smaller extrapolation factor.

After the extrapolation to full rapidity, we find the total production cross section accompanied by mutual nuclear excitation to be $\sigma_{\text{coh}}(XnXn, \text{full-}y) = 10.5 \pm 1.5$ (stat.) ± 1.6 (syst.) mb, the total production cross section accompanied by a single nuclear excitation to be $\sigma_{\text{coh}}(0nXn, \text{full-}y) = 31.8 \pm 5.2$ (stat.) ± 3.9 (syst.) mb, and the total production cross section with no accompanying excitation to be $\sigma_{\text{coh}}(0n0n, \text{full-}y) = 78 \pm 14$ (stat.) ± 13 (syst.) mb. The individual cross sections are summarized in Table II.

Adding these three cross sections together yields the total coherent cross section at $\sqrt{s_{NN}} = 62$ GeV, $\sigma_{\text{coh}}(\text{AuAu} \rightarrow \text{Au}^{(*)}\text{Au}^{(*)}\rho^0) = 120 \pm 15$ (stat.) ± 22 (syst.) mb.

We considered several sources for systematic errors as was done in previous work reported in Ref. [10]. The biggest contributions to the overall uncertainty in the cross section measurement come from the luminosity measurements, the acceptance corrections, and the extrapolation to the full rapidity range which exhibits strong model dependence. The different methods of combinatorial background estimation gave cross sections which differ by less than 3 %. The contribution due to the luminosity measurement is 10 %, and the contribution due to the various cuts is approximately 7 %. The error due to the extrapolation to the full phase space is 6 %. Different models used to describe the background yielded a 5 % systematic error.

The two data sets taken with triggers A and B were used to cross check measured cross sections and to study systematic effects of different trigger requirements on measured luminosity and acceptance corrections.

The measured cross sections are summarized in Table II and compared with previous results at $\sqrt{s_{NN}} = 130$ and 200 GeV [10, 11]. The cross-section ratio for the 200 GeV and 62 GeV data is $R = \sigma(200\text{GeV})/\sigma(62.4\text{GeV}) = 4.4 \pm 0.6$, where we have added the systematic and statistical errors in quadrature, neglecting the partial correlation between the systematic errors at the two energies. The 130 GeV data have large errors, but we find $R = \sigma(130\text{GeV})/\sigma(62.4\text{GeV}) = 3.8 \pm 1.9$. These ratios are much larger than was previously found for $R = \sigma(200\text{GeV})/\sigma(130\text{GeV}) = 1.15 \pm 0.6$, and point to a considerably steeper rise in cross-section with energy, at least as steeply as predicted by the models.

Figure 4 compares the measured cross section at three different energies with the aforementioned four theoretical models [3, 4, 7]. For the KN model, the STARlight code was used to predict the energy dependence of the cross-section [21]. For the other models, we relied on personal communications from the authors to get the energy dependence [23, 24].

The rise in cross-section is smaller than is predicted by the KN and FSZ models, which both use Glauber calculations to predict ratios around 6.1 It is closer to the IPSAT-GM and IIM-GM predictions of 3.5 and 4.3 respectively. However, for these models, the extrapolation from $|y| < 1$ to all rapidities would be considerably smaller for the IPSAT and IIM models; since the extrapolation factor depends on the energy, the comparison should be treated with some caution. For the two Glauber models, the comparison should be more straightforward, although, at 62.4 GeV, the impact parameters are smaller than at 200 GeV, and uncertainties due to the nuclear geometry become more important.

IV. CONCLUSION

Coherent and incoherent photoproduction of ρ^0 mesons accompanied by the mutual excitation of the beam ions has been measured in relativistic AuAu collisions at $\sqrt{s_{NN}} = 62.4$ GeV with the STAR detector at RHIC. The ρ^0 production cross section for the events with mutual excitation ($XnXn$) measured with the minimum bias trigger is 10.5 ± 1.5 (stat.) ± 1.6 (syst.) mb and the total coherent cross section $\sigma_{\text{coh}}(\text{AuAu} \rightarrow \text{Au}^{(*)}\text{Au}^{(*)}\rho^0) = 120 \pm 15$

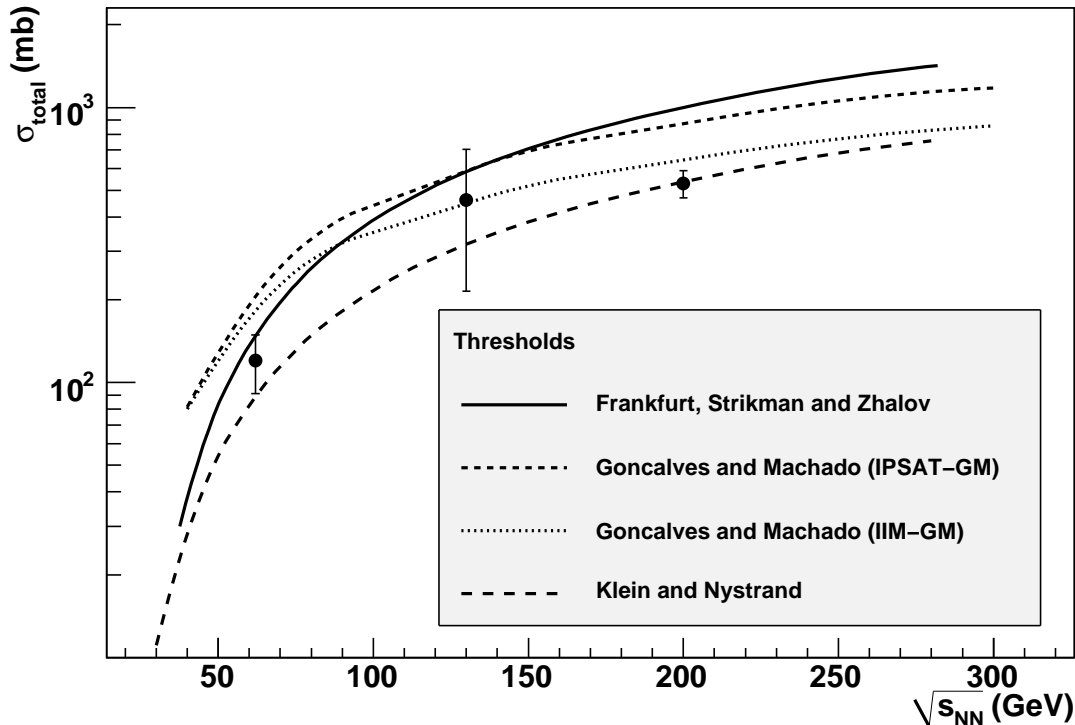


FIG. 4: Comparison of theoretical predictions to the measured total cross section for coherent ρ^0 production as a function of $\sqrt{s_{NN}}$. The measured cross section is based on the dataset collected with trigger B. The error bars show the sum of the statistical and systematic uncertainties. See text for details.

(stat.) \pm 22 (syst.) mb. The ratio of incoherently to coherently produced ρ^0 is 0.20 ± 0.08 (stat.) \pm 0.08 (syst.), in agreement with previous measurements at higher energies.

The increase in cross section shown by the measurements at 62.4, 130 and 200 GeV is close to the predictions of IIM-GM and somewhat below the predictions of the Glauber theory models.

Acknowledgments

We thank Mark Strikman, M. Zhalov and M. V. T. Machado for providing theoretical photoproduction cross-sections at 62.4 and 130 GeV. We thank the RHIC Operations Group and RCF at BNL, the NERSC Center at LBNL and the Open Science Grid consortium for providing resources and support. This work was supported in part by the Offices of NP and HEP within the U.S. DOE Office of Science, the U.S. NSF, the Sloan Foundation, the DFG cluster of excellence ‘Origin and Structure of the Universe’ of Germany, CNRS/IN2P3, FAPESP CNPq of Brazil, Ministry of Ed. and Sci. of the Russian Federation, NNSFC, CAS, MoST, and MoE of China, GA and MSMT of the Czech Republic, FOM and NWO of the Netherlands, DAE, DST, and CSIR of India, Polish Ministry of Sci. and Higher Ed., Korea Research Foundation, Ministry of Sci., Ed. and Sports of the Rep. Of Croatia, and RosAtom of Russia.

-
- [1] C. F. v. Weizsäcker, Z. Phys. **88**, 612 (1934), E.J. Williams, Phys. Rev. **45**, 729 (1934).
 - [2] G. Baur *et al.*, Phys. Rep. **364**, 359 (2002); F. Krauss, M. Greiner and G. Soff, Prog. Part. Nucl. Phys. **39**, 503 (1997); C. Bertulani, S. Klein and J. Nystrand; Annu. Rev. Nucl. Part. Sci. **55**, 271 (2005).
 - [3] S. Klein and J. Nystrand, Phys. Rev. **C60**, 014903 (1999); A. J. Baltz, S. R. Klein and J. Nystrand, Phys. Rev. Lett. **89**, 012301 (2002).
 - [4] L. Frankfurt, M. Strikman and M. Zhalov, Phys. Rev. **C67**, 034901 (2003).

- [5] L. Frankfurt, M. Strikman and M. Zhalov, Phys. Lett. **B537**, 51 (2002).
- [6] E. Iancu, K. Itakura and S. Munier, Phys. Lett. **B590**, 199 (2004).
- [7] V. P. Gonçalves and M. V. T. Machado, Eur. Phys. J. **C40**, 519 (2005).
- [8] V.N. Gribov and L.N. Lipatov. Sov. J. Nucl. Phys. 15, 438 (1972).
- [9] V. P. Gonçalves *et al.*, Phys. Lett. B **643**, 273 (2006).
- [10] B. I. Abelev *et al.*, Phys. Rev. **C77**, 034910 (2008).
- [11] C. Adler *et al.*, Phys. Rev. Lett. **89**, 272302 (2002).
- [12] M. Anderson *et al.*, Nucl. Instrum. Methods **A499**, 659 (2003); M. Anderson *et al.*, Nucl. Instrum. Methods **A499**, 679 (2003).
- [13] F. S. Bieser *et al.*, Nucl. Instrum. Methods **A499**, 766 (2003).
- [14] C. Adler *et al.*, Nucl. Instrum. Methods **A470**, 488 (2001).
- [15] V. Morozov, Ph.D. Thesis, UC Berkeley, (2003).
- [16] J. Adams *et al.*, Phys. Rev. **C70**, 044901 (2004).
- [17] B. I. Abelev *et al.*, Phys. Rev. Lett. **102**, 112301 (2009).
- [18] B. I. Abelev *et al.*, Phys. Rev. **C79**, 034909 (2009).
- [19] P. Söding, Phys. Lett. **19**, 702 (1966).
- [20] W.-M. Yao *et al.*, J. Phys. **G33**, 1 (2006).
- [21] The latest C++ version of STARlight is available at <http://projects.hepforge.org/starlight/>.
- [22] J. Nystrand and S. Klein, nucl-ex/9811007.
- [23] M. Zhalov, personal communication, 2010.
- [24] M. V. T. Machado, personal communication, 2010.